

Tailoring Photocurrent in Weyl Semimetals via Intense Laser Irradiation

Amar Bharti¹ and Gopal Dixit^{1,2,3,*}

¹*Department of Physics, Indian Institute of Technology Bombay, Powai, Mumbai 400076, India*

²*Center for Computational Sciences, University of Tsukuba, Tsukuba 305-8577, Japan*

³*Max-Born Institut, Max-Born Straße 2A, 12489 Berlin, Germany*

(Dated: October 30, 2023)

Abstract

Generating and tailoring photocurrent in topological materials has immense importance in fundamental studies and the technological front. Present work introduces a universal method to generate ultrafast photocurrent in *both* inversion-symmetric and inversion-broken Weyl semimetals with degenerate Weyl nodes at the Fermi level. Our approach harnesses the asymmetric electronic population in the conduction band induced by an intense *single-color* circularly polarized laser pulse. It has been found that the induced photocurrent can be tailored by manipulating helicity and ellipticity of the employed laser. Moreover, our approach generates photocurrent in realistic situations when the Weyl nodes are positioned at different energies and have finite tilt along a certain direction. Present work adds a new dimension on practical applications of Weyl semimetals for optoelectronics and photonics-based quantum technologies.

Weyl semimetals are topological materials that have demonstrated the potential to convert light into electricity efficiently. The superiority of the Weyl semimetal over many materials in generating photocurrent in the infrared region has been established experimentally¹. In addition, ultrafast photocurrent from Weyl semimetals can be a source of terahertz radiation^{2,3}. Moreover, photocurrent emerges as a quintessential probe of the topological properties of quantum materials⁴⁻⁶, including device characterization⁷. Thus, recent developments in producing photocurrent from Weyl semimetals make them a central focus for various applications in optoelectronics, detection, and sensing to name but a few⁸⁻¹⁴.

Asymmetric population distribution of the electronic excitations in Weyl semimetal renders a finite photocurrent – photogalvanic effect – which can be realized in various ways, such as the chiral magnetic effect¹⁵⁻¹⁷, via transfer of angular momentum of light to the Weyl nodes¹⁸, and nonlinear optical responses in the perturbative regime^{6,19-26}. It has been shown that the inversion-broken Weyl semimetal with gyrotropic symmetry produces second-order nonlinear optical responses – injection and shift currents – which lead to a colossal photocurrent in TaAs^{1,27-29}. In addition, photocurrent can exhibit a sign flip with the change in the helicity of the circularly polarized light^{18,30,31}. The broken mirror-symmetry of Weyl nodes is a key reason behind helicity-sensitive photoresponse in the inversion-broken Weyl semimetals³²⁻³⁴. So far, the majority of the work on photocurrent is focused on inversion-broken Weyl semimetals with various tilts and crystal symmetries, as in the recent one in an inversion-symmetric Weyl semimetal³⁵. Thus, a universal method to generate photocurrent from both inversion-symmetric and inversion-broken Weyl semimetals that does not rely on such materials’ symmetry details is lacking.

It is a commonly accepted notion that the single-color circularly polarized light fails to generate photocurrent in Weyl semimetals with mirror-symmetric Weyl nodes. While each Weyl node generates current depending on its chirality, the currents in a chiral pair of the mirror-symmetric Weyl nodes cancel each other. In contrast to this accepted notion, we unequivocally demonstrate that a single-color circularly polarized light is able to generate photocurrent in mirror-symmetric Weyl semimetals. Our approach does not rely on the system’s symmetry as it is equally applicable to both inversion-symmetric and inversion-broken Weyl semimetals with isotropic band dispersion and even with all Weyl nodes at the Fermi level. Recently, bicircular laser pulses have been proposed for generating photocurrent in two- and three-dimensional materials, including Weyl semimetal, described by

a linear anisotropic Hamiltonian^{36,37}. However, a single-color laser based photocurrent, with relatively easy experimental setup, is highly desirable for practical purposes. Few-cycle carrier-envelope phase stabilized linearly polarized laser can induce photocurrent as shown for graphene^{38,39}. However, such photocurrent cancels out if the phase is not stabilized, outweighing its applicability. Our approach is also robust against such carrier-envelope phase stabilization. We employ three- and six-cycle laser pulses in the mid-infrared regime to generate photocurrents whose direction and magnitude can be tailored by the phase of the circular pulse. Moreover, it is observed that the photocurrent in an inversion-symmetric Weyl semimetal is sensitive to the helicity and ellipticity of the laser pulse.

We start our discussion by writing the Hamiltonian of Weyl semimetals as $\mathcal{H}(\mathbf{k}) = \mathbf{d}(\mathbf{k}) \cdot \boldsymbol{\sigma}$, with $\boldsymbol{\sigma}$'s being the Pauli matrices. Expressions of the three components of $\mathbf{d}(\mathbf{k})$ for an inversion-symmetric Weyl semimetal are^{40,41}

$$\mathbf{d}(\mathbf{k}) = [t \sin(k_x a), t \sin(k_y a), t\{\cos(k_z a) - \cos(k_0 a) + 2 - \cos(k_x a) - \cos(k_y a)\}], \quad (1)$$

and for an inversion-broken Weyl semimetal read as

$$\begin{aligned} \mathbf{d}(\mathbf{k}) = & [t\{\cos(k_0 a) - \cos(k_y a) + \mu[1 - \cos(k_z a)]\}, t \sin(k_z a), \\ & t\{\cos(k_0 a) - \cos(k_x a) + \mu[1 - \cos(k_z a)]\}]. \end{aligned} \quad (2)$$

Here, k_0 determines the position of the Weyl nodes, which are considered as $\pi/(2a)$ for both Weyl semimetals. The Weyl nodes for inversion-symmetric and inversion-broken systems are situated at $\mathbf{k} = [0, 0, \pm\pi/(2a)]$ and $\mathbf{k} = [\pm\pi/(2a), \pm\pi/(2a), 0]$, respectively. A simple cubic crystal structure is considered with lattice parameter $a = 6.28 \text{ \AA}$ and isotropic hopping parameter $t = 1.8 \text{ eV}$ in Eqs. (1) and (2). Moreover, a dimensionless parameter $\mu = 2$ is used in Eq. (2). Energy band dispersions corresponding to Eqs. (1) and (2) are shown in Figs. S1 and S2 in Ref.⁴², respectively.

The vector potential of the circularly polarized laser is written as $\mathbf{A}(t) = A_0 \text{Re}\{e^{i\omega t + \phi} \hat{\mathbf{e}}_{\pm}\}$, where $\hat{\mathbf{e}}_{\pm} = (\hat{\mathbf{e}}_x \pm i\epsilon \hat{\mathbf{e}}_y)$ corresponds to left- and right-handed circularly polarized laser pulse with ellipticity $\epsilon = 1$. The subcycle phase of the laser pulse is denoted by ϕ , which controls the orientation of the Lissajous profile of the laser. A laser pulse having a sine-squared envelope with wavelength $3.2 \text{ }\mu\text{m}$ and pulse duration ranging from ~ 35 to 70 fs is employed to generate photocurrent. The density-matrix-based approach is used to simulate laser-driven dynamics in Weyl semimetals as discussed in Refs.^{43–46}. The photocurrent originates from

the population asymmetry and can be written as ⁴⁷

$$\mathbf{J}(t) = \int_{\mathbf{k}} d\mathbf{k} [\rho(\mathbf{k}) - \rho(-\mathbf{k})] \frac{\partial \mathcal{E}(\mathbf{k})}{\partial \mathbf{k}}, \quad (3)$$

where $\mathbf{J}(t)$ is the total current, ρ is the residual population density after the end of the laser pulse, and $\mathcal{E}(\mathbf{k})$ is the energy dispersion in a Weyl semimetal.

Let us analyze results for an inversion-symmetric Weyl semimetal, which exhibits a finite photocurrent along x and y directions after the end of the laser pulse as shown in Fig. 1(a). As the helicity of the laser changes from right to left, the sign of the photocurrent along the y direction flips from negative to positive as evident from Fig. 1(b). To unravel the underlying mechanism for the flip, we analyzed the Lissajous profile of the vector potential in the polarization plane as shown in the insets. The change in the Lissajous curve with a change in the helicity is a primary reason for the sign flips along y direction. This shows that the photocurrent is susceptible to the profile of the laser pulse. At this juncture, it is pertinent to know how the photocurrent is sensitive to the phase of the laser pulse. To this end, we investigate variation in the total photocurrent and its components with respect to the phase.

Figure 1(c) shows the insensitivity of the photocurrent with respect to ϕ , which concludes that phase stabilization is not a prerequisite to generate photocurrent in Weyl semimetal. However, the x component (J_x) changes from a positive to a negative value as ϕ changes from 0 to π , including zero at $\phi = \pi/2$ [see Fig. 1(d)]. Both helicities display similar behavior for J_x , whereas the y component (J_y) exhibits an opposite trend as the helicity is reversed from left and right, except $\phi = 0$ and π where it is zero [see Fig. 1(e)]. Analysis of Fig. 1 raises a crucial question about factors determining the nonzero photocurrent and its components.

The residual population in the conduction band around a Weyl node after the end of the laser is presented in Fig. 2. Owing to the zero band-gap nature of the Weyl node, the region around the node is significantly populated, which decreases rapidly as we move away from the origin. Population about the $k_x = 0$ plane is significantly asymmetric, which in results nonzero photocurrent along this direction as $\rho(k_x) \neq \rho(-k_x)$ for both helicities. However, the population exhibits mirror symmetry about the $k_y = 0$ plane for $\phi = 0$, which in results in zero photocurrent for both helicities as evident from Figs. 1(e), 2(a) and 2(b). A change in ϕ from 0 to $\pi/4$ induces asymmetry along $k_y = 0$, which generates finite photocurrent as reflected from Figs. 2(a) and 2(b). In addition, the direction of the induced asymmetry

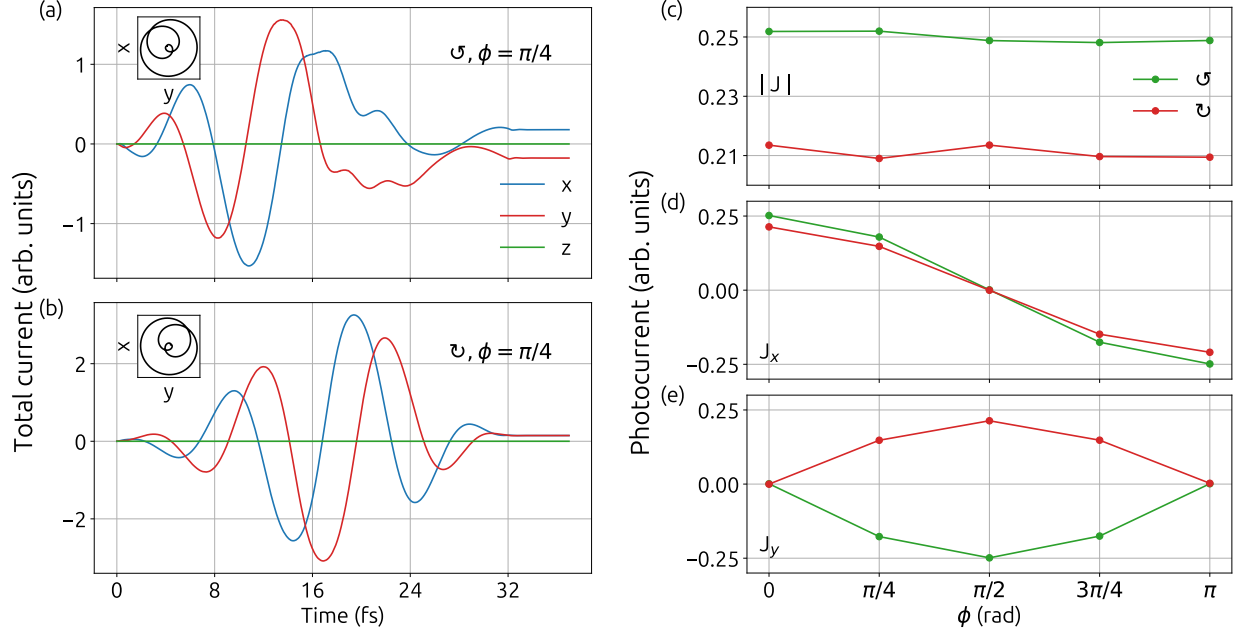


FIG. 1. Total photocurrent in an inversion-symmetric Weyl semimetal induced by (a) left-handed and (b) right-handed circularly polarized laser with phase $\phi = \pi/4$. The Lissajous curve in the xy plane is shown in respective insets. Variations in (c) the photocurrent, (d) its x (J_x), and (e) y (J_y) components with respect to the phase. These results are obtained for a three-cycle circularly polarized laser pulse with ~ 32 fs duration, $3.2 \mu\text{m}$ wavelength, and 10^{11} W/cm^2 intensity.

along $k_y = 0$ flips as we change the helicity from left and right, which results in a sign change in J_y as shown in Fig. 1(e). Thus, observations in Figs. 1 and 2 are consistent with Eq. (3).

One of the striking features of Fig. 2 is the extent of the asymmetries along $k_x = 0$ and $k_y = 0$ planes, which are significantly different for both helicities. Recently, it has been shown that the electronic excitation from the nonlinear part of the band dispersion can effectuate the helicity-dependent population in an inversion-symmetric Weyl semimetal⁴⁸. Therefore, owing to the unique coupling of the circularly polarized laser with the Weyl semimetal, the residual population along k_z , integrated along other directions, is sensitive to the laser's helicity⁴⁸. Thus, the helicity-sensitive population asymmetry leads to different photocurrent for the left- and right-handed laser pulses as shown in Fig. 1.

So far, we have discussed the results of the three-cycle laser pulse. It is known that the vector potential can be nonzero when the electric field is zero for a few-cycle laser pulse with stabilized carrier-envelope phase. The nonzero vector potential can induce asymmetric population and photocurrent in graphene, as discussed in Refs.^{38,39}. Moreover, the resultant

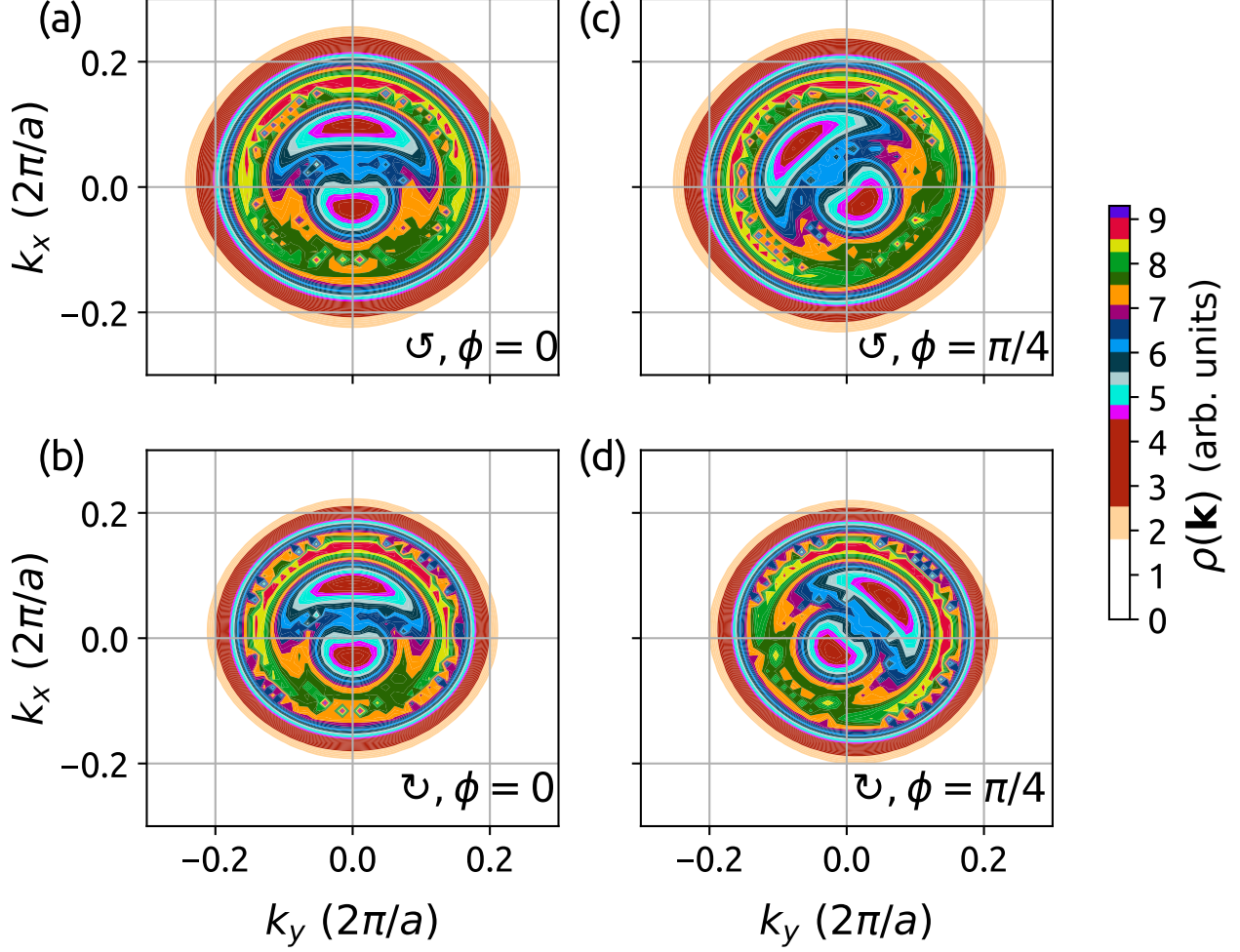


FIG. 2. Residual population in the conduction band of an inversion-symmetric Weyl semimetal after the end of the (a) left-handed, and (b) right-handed circularly polarized laser with $\phi = 0$. (c) and (d) are, respectively the same as (a) and (b) for $\phi = \pi/4$. Weyl nodes are situated at $\mathbf{k} = [0, 0, \pm\pi/(2a)]$ according to Eq. (1). Population along k_z direction is integrated in all cases. Laser parameters are identical to Fig. 1.

asymmetric population can also yield valley polarization in two-dimensional materials^{49–51}. Thus, it is natural to ask about the robustness of our results with the pulse duration. Generating photocurrent in Weyl semimetals via relatively long laser pulse in mid-infrared regime is highly desirable for numerous practical applications^{6,19–24}.

Towards that end, let us increase the pulse duration from $\simeq 30$ to 65 fs by changing the number of cycles from three to six while keeping the intensity constant. In this case, a finite photocurrent with a relatively smaller magnitude is observed. It is found that the intensity

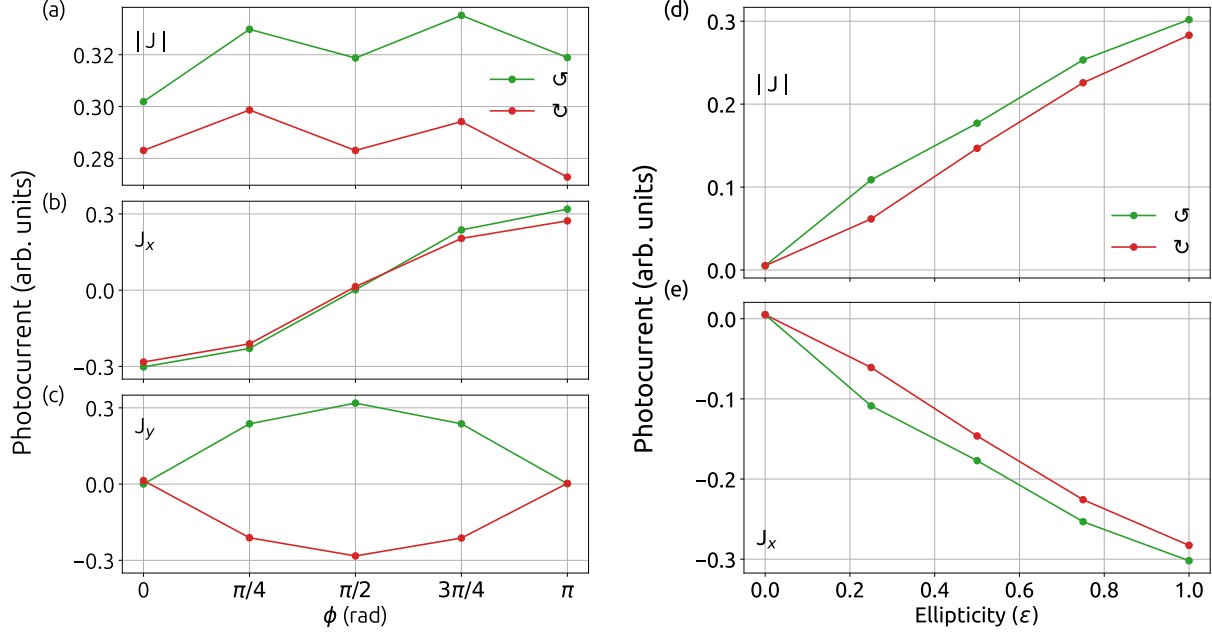


FIG. 3. Variations in (a) the total photocurrent, (b) its x (J_x), and (c) y (J_y) components with respect to ϕ for an inversion-symmetric Weyl semimetal. Sensitivity of (d) the photocurrent and (e) J_x with respect to the ellipticity of the laser for $\phi = 0$. The laser pulse consists of six cycles with 5×10^{11} W/cm² intensity and 3.2 μm wavelength.

needs to be increased by five times to make the magnitude of the photocurrent comparable for three- and six-cycle pulses [see Fig. 3(a)]. On comparing Figs. 1(c) and 3(a), it is evident that an increase in intensity leads to a reduction in the contrast between the photocurrent for different helicity. The reduction in the contrast can be attributed to the underlying mechanism of the helicity-dependent asymmetric population, which relies on the resonant excitation at various \mathbf{k} and thus reduces the asymmetry with an increase in intensity⁴⁸.

In contrast to the three-cycle pulse, J_x transits from negative to positive magnitude as ϕ changes from 0 to π , whereas J_y exhibits similar behavior for three- and six-cycle pulses [see Figs. 3(b) and 3(c)]. Note that the photocurrent can be positive or negative based on whether $-\mathbf{k}$ or \mathbf{k} is more populated, which depends on the intensity and pulse duration³⁹. The photocurrent is not only sensitive to the pulse duration but also to the ellipticity of the laser pulse, as shown in Fig. 3(d) for $\phi = 0$. Photocurrent monotonically reduces to zero as the ellipticity changes from one (circular) to zero (linear) for both helicities. Similar observations can be made for J_x from Fig. 3(e). Note that J_y is zero for $\phi = 0$. The generated photocurrent is nonperturbative in nature as evident from its scaling with laser's intensity

[see Fig. S3⁴²]. Our analysis establishes that a laser pulse with definite chirality, but nonzero ellipticity, is able to engender photocurrent in an inversion-symmetric Weyl semimetal, which also encapsulates a unique coupling of chiral light with Weyl semimetal⁴⁸. Our approach is equally applicable to realistic situations when the Weyl nodes are nondegenerate [see Fig. S4⁴²], situated at different energies, and have tilt along certain direction [see Fig. S5⁴²]. In addition, our method produces photocurrent of the same order [see Fig. S6⁴²] as the one reported by Morimoto and coworkers using bicircular counter-rotating laser pulses³⁶.

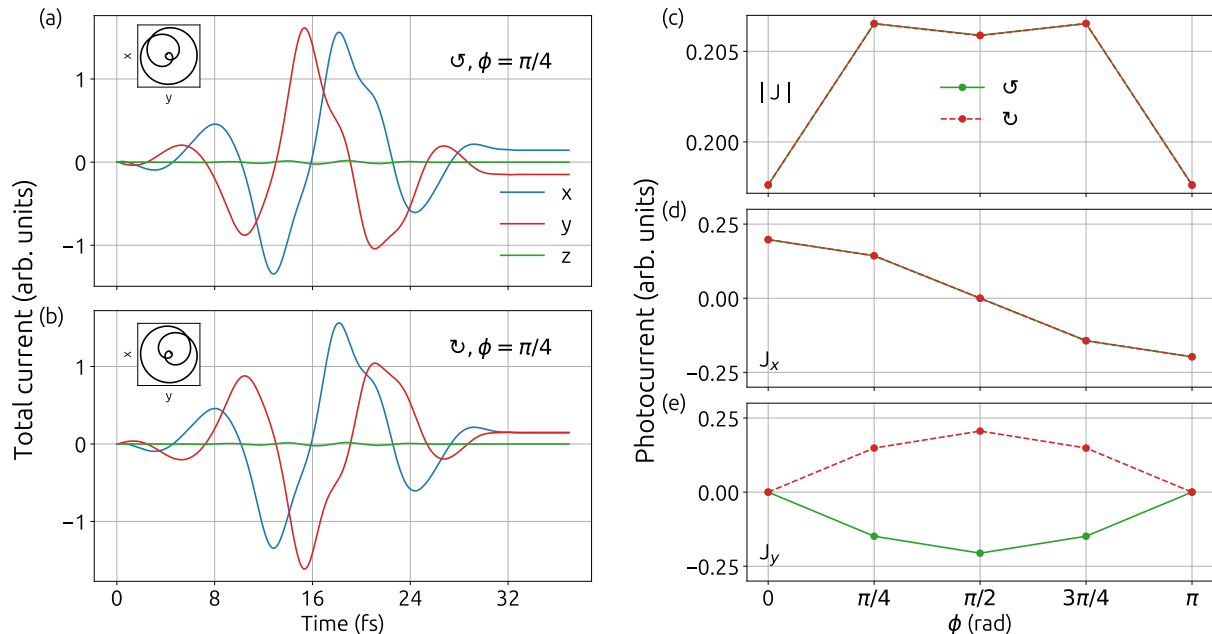


FIG. 4. Same as Fig. 1 for an inversion-broken Weyl semimetal as described by the Hamiltonian in Eq. (2).

After demonstrating the photocurrent generation in an inversion-symmetric Weyl semimetal, let us focus our discussion to inversion-broken Weyl semimetal. Figure 4 presents finite photocurrent in an inversion-broken Weyl semimetal driven by a circularly polarized laser. By the virtue of the Lissajous profile flip, the photocurrent along y direction flips its sign as the laser's helicity changes for $\phi = \pi/4$ [see Figs. 4(a) and 4(b)]. The total photocurrent does not change significantly with variation in ϕ and is identical for both helicities as shown in Fig. 4(c). Similar to an inversion-symmetric case, J_x changes its magnitude from positive to negative as ϕ changes from 0 to π [see Fig. 4(d)], and J_y remains either positive or negative depending on the helicity except at $\phi = 0$ and π [see Fig. 4(e)]. Thus, the behavior of the photocurrent and its components are robust with respect to ϕ . Note that there is a finite

photocurrent in the plane of polarization for other polarization directions of the laser, and can be tailored by changing ϕ .

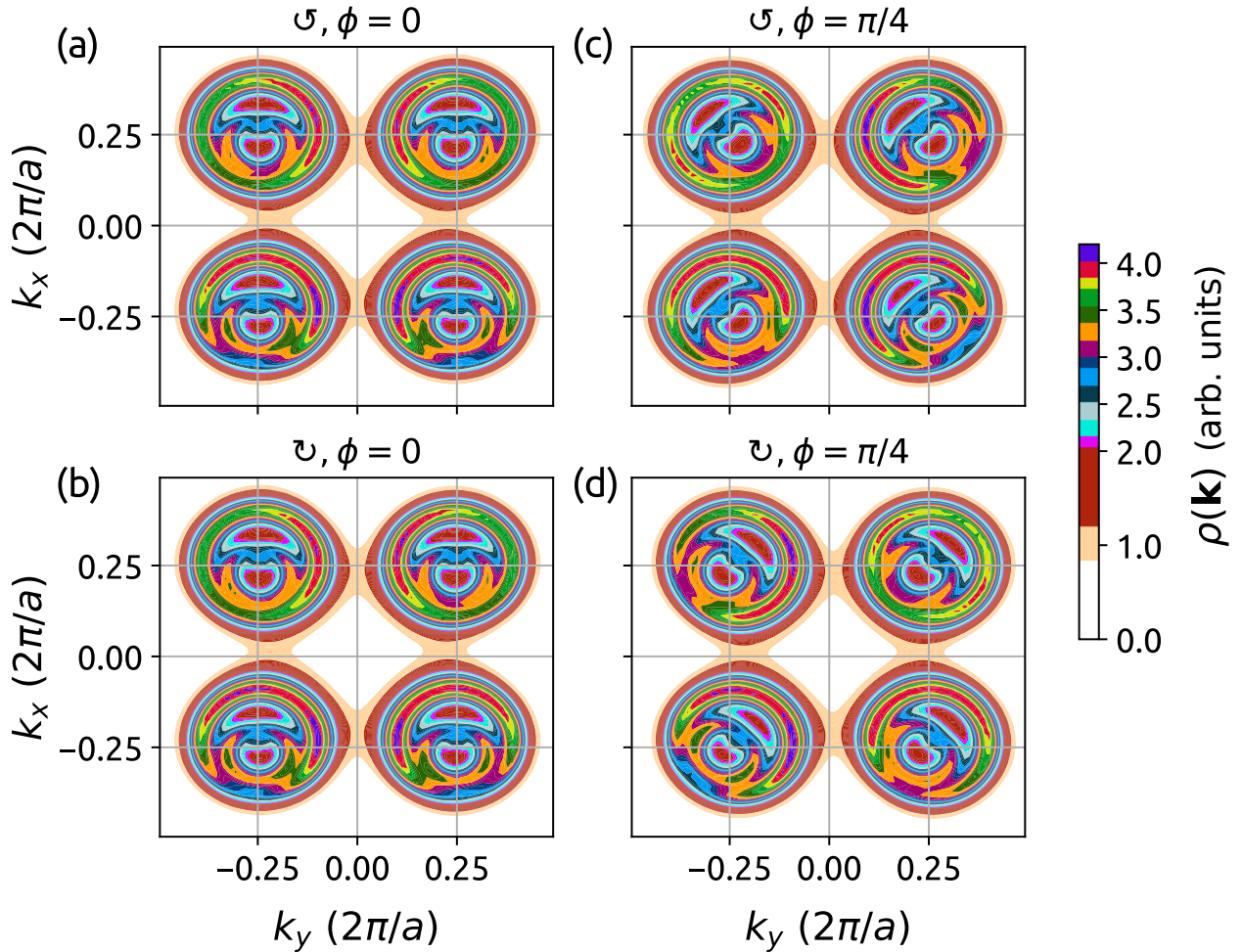


FIG. 5. Same as Fig. 2 for an inversion-broken Weyl semimetal.

We also analyze the residual population in the conduction band to corroborate the photocurrent's results in Fig. 4. Significant population around four Weyl nodes at $\mathbf{k} = [\pm\pi/(2a), \pm\pi/(2a), 0]$ is observed as shown in Fig. 5. Population is asymmetric in nature with respect to $k_x = 0$ plane for $\phi = 0$ and exhibits $k_y = 0$ as a plane of reflection, which results in nonzero (zero) photocurrent along x (y) axis. Reflection symmetry about $k_y = 0$ plane is lost as ϕ changes to $\pi/4$ [see Figs. 5(c) and 5(d)], which results in nonzero photocurrent along this direction as evident from Fig. 4(e). In addition, the population corresponding to both helicities are identical, which is in contrast to the one observed for an inversion-symmetric Weyl semimetal.

To summarize, we introduce a robust and universal method to generate photocurrent in

both inversion-symmetric and inversion-broken Weyl semimetals using a single-color circularly polarized light. Both Weyl semimetals have degenerate Weyl nodes at Fermi level. We unequivocally show that phase stabilization is not a prerequisite to generate photocurrent in both types of the Weyl semimetals as the generated photocurrent is insensitive to the phase of the laser pulse. Photocurrent in an inversion-symmetric Weyl semimetal is sensitive to the helicity of the laser as the left-handed circularly polarized laser yields more photocurrent in comparison to the right-handed laser. Moreover, the components of the photocurrent in an inversion-symmetric Weyl semimetal are also sensitive to the helicity, whereas only the y component exhibits sensitivity in case of an inversion-broken Weyl semimetal. In addition, the strength of the photocurrent reduces as the ellipticity of the laser changes from circular to linear. It is anticipated that the measurement of the photocurrent can quantify the coupling of spin-angular momentum of light with nonlinear band dispersion in Weyl semimetals. Our introduced method can be extended to other topological materials for their widespread applications in optoelectronics and photonics.

G. D. acknowledges fruitful discussions with Misha Ivanov (MBI, Berlin) and Kazuhiro Yabana (Tsukuba University). G. D. acknowledges financial support from SERB India (Project No. MTR/2021/000138).

* gdixit@phy.iitb.ac.in

- ¹ G. B. Osterhoudt, L. K. Diebel, M. J. Gray, X. Yang, J. Stanco, X. Huang, B. Shen, N. Ni, P. J. Moll, Y. Ran, et al., *Nature Materials* **18**, 471 (2019).
- ² N. Sirica, R. Tobey, L. Zhao, G. Chen, B. Xu, R. Yang, B. Shen, D. Yarotski, P. Bowlan, S. Trugman, et al., *Physical Review Letters* **122**, 197401 (2019).
- ³ Y. Gao, S. Kaushik, E. Philip, Z. Li, Y. Qin, Y. Liu, W. Zhang, Y. Su, X. Chen, H. Weng, et al., *Nature Communications* **11**, 720 (2020).
- ⁴ Y. Pan, Q.-Z. Wang, A. L. Yeats, T. Pillsbury, T. C. Flanagan, A. Richardella, H. Zhang, D. D. Awschalom, C.-X. Liu, and N. Samarth, *Nature Communications* **8**, 1037 (2017).
- ⁵ Y. Zhang, T. Holder, H. Ishizuka, F. de Juan, N. Nagaosa, C. Felser, and B. Yan, *Nature Communications* **10**, 3783 (2019).
- ⁶ H. Wang and X. Qian, *npj Computational Materials* **6**, 199 (2020).
- ⁷ Q. Ma, R. Krishna Kumar, S.-Y. Xu, F. H. Koppens, and J. C. Song, *Nature Reviews Physics* **5**, 170 (2023).
- ⁸ Q. Wang, J. Zheng, Y. He, J. Cao, X. Liu, M. Wang, J. Ma, J. Lai, H. Lu, S. Jia, et al., *Nature Communications* **10**, 5736 (2019).
- ⁹ L. Luo, D. Cheng, B. Song, L.-L. Wang, C. Vaswani, P. Lozano, G. Gu, C. Huang, R. H. Kim, Z. Liu, et al., *Nature Materials* **20**, 329 (2021).
- ¹⁰ J. Ma, B. Cheng, L. Li, Z. Fan, H. Mu, J. Lai, X. Song, D. Yang, J. Cheng, Z. Wang, et al., *Nature Communications* **13**, 5425 (2022).
- ¹¹ Y.-X. Wang, X.-Y. Zhang, C. Li, X. Yao, R. Duan, T. K. Graham, Z. Liu, F. Tafti, D. Broido, Y. Ran, et al., *Nature Physics* **19**, 507 (2023).
- ¹² A. Bharti and G. Dixit, *Physical Review B* **107**, 224308 (2023).
- ¹³ J. Liu, F. Xia, D. Xiao, F. J. Garcia de Abajo, and D. Sun, *Nature materials* **19**, 830 (2020).
- ¹⁴ J. Ma, Q. Gu, Y. Liu, J. Lai, P. Yu, X. Zhuo, Z. Liu, J.-H. Chen, J. Feng, and D. Sun, *Nature Materials* **18**, 476 (2019).
- ¹⁵ K. Taguchi, T. Imaeda, M. Sato, and Y. Tanaka, *Physical Review B* **93**, 201202 (2016).
- ¹⁶ S. Kaushik, D. E. Kharzeev, and E. J. Philip, *Physical Review B* **99**, 075150 (2019).
- ¹⁷ S. Kaushik, D. E. Kharzeev, and E. J. Philip, *Physical Review Research* **2**, 042011 (2020).

- ¹⁸ F. De Juan, A. G. Grushin, T. Morimoto, and J. E. Moore, *Nature Communications* **8**, 15995 (2017).
- ¹⁹ H. Watanabe and Y. Yanase, *Physical Review X* **11**, 011001 (2021).
- ²⁰ S. Heidari and R. Asgari, *Physical Review B* **106**, 195148 (2022).
- ²¹ L. Golub, E. L. Ivchenko, and B. Spivak, *JETP Letters* **105**, 782 (2017).
- ²² N. Sirica, P. P. Orth, M. Scheurer, Y. Dai, M.-C. Lee, P. Padmanabhan, L. Mix, S. Teitelbaum, M. Trigo, L. Zhao, et al., *Nature Materials* **21**, 62 (2022).
- ²³ L. Golub and E. Ivchenko, *Physical Review B* **98**, 075305 (2018).
- ²⁴ H. Ishizuka, T. Hayata, M. Ueda, and N. Nagaosa, *Physical Review Letters* **117**, 216601 (2016).
- ²⁵ Y. Zhang, H. Ishizuka, J. van den Brink, C. Felser, B. Yan, and N. Nagaosa, *Physical Review B* **97**, 241118 (2018).
- ²⁶ L. Gao, Z. Addison, E. Mele, and A. M. Rappe, *Physical Review Research* **3**, L042032 (2021).
- ²⁷ T. Morimoto and N. Nagaosa, *Science Advances* **2**, e1501524 (2016).
- ²⁸ J. Orenstein, J. Moore, T. Morimoto, D. Torchinsky, J. Harter, and D. Hsieh, *Annual Review of Condensed Matter Physics* **12**, 247 (2021).
- ²⁹ Q. Ma, A. G. Grushin, and K. S. Burch, *Nature Materials* **20**, 1601 (2021).
- ³⁰ C.-K. Chan, N. H. Lindner, G. Refael, and P. A. Lee, *Physical Review B* **95**, 041104 (2017).
- ³¹ E. König, H.-Y. Xie, D. Pesin, and A. Levchenko, *Physical Review B* **96**, 075123 (2017).
- ³² Q. Ma, S.-Y. Xu, C.-K. Chan, C.-L. Zhang, G. Chang, Y. Lin, W. Xie, T. Palacios, H. Lin, S. Jia, et al., *Nature Physics* **13**, 842 (2017).
- ³³ D. Rees, K. Manna, B. Lu, T. Morimoto, H. Borrmann, C. Felser, J. Moore, D. H. Torchinsky, and J. Orenstein, *Science advances* **6**, eaba0509 (2020).
- ³⁴ Z. Ni, K. Wang, Y. Zhang, O. Pozo, B. Xu, X. Han, K. Manna, J. Paglione, C. Felser, A. G. Grushin, et al., *Nature Communications* **12**, 154 (2021).
- ³⁵ D. Hamara, G. F. Lange, F. N. Kholid, A. Markou, C. Felser, R.-J. Slager, and C. Ciccarelli, *arXiv preprint arXiv:2302.07286* (2023).
- ³⁶ Y. Ikeda, S. Kitamura, and T. Morimoto, *Physical Review Letters* **131**, 096301 (2023).
- ³⁷ O. Neufeld, N. Tancogne-Dejean, U. De Giovannini, H. Hübener, and A. Rubio, *Physical Review Letters* **127**, 126601 (2021).
- ³⁸ T. Higuchi, C. Heide, K. Ullmann, H. B. Weber, and P. Hommelhoff, *Nature* **550**, 224 (2017).
- ³⁹ X. Zhang, E. Wu, H. Du, H. Guo, and C. Liu, *Optics Express* **30**, 37863 (2022).

- ⁴⁰ B. Sadhukhan and T. Nag, *Physical Review B* **103**, 144308 (2021).
- ⁴¹ A. Menon, S. Chattopadhyay, and B. Basu, *Physical Review B* **104**, 075129 (2021).
- ⁴² See Supplemental Material at <http://link.aps.org/supplemental/> for Energy band dispersion, theoretical methodology, scaling of photocurrent with laser's intensity, effect of energy splitting of Weyl nodes from Fermi level on photocurrent, effect of tilt of the Weyl nodes on photocurrent, and photocurrent due to bicircular counter-rotating laser fields.
- ⁴³ M. Mrudul and G. Dixit, *Physical Review B* **103**, 094308 (2021).
- ⁴⁴ J. Wilhelm, P. Grössing, A. Seith, J. Crewse, M. Nitsch, L. Weigl, C. Schmid, and F. Evers, *Physical Review B* **103**, 125419 (2021).
- ⁴⁵ N. Rana, M. Mrudul, D. Kartashov, M. Ivanov, and G. Dixit, *Physical Review B* **106**, 064303 (2022).
- ⁴⁶ A. Bharti, M. Mrudul, and G. Dixit, *Physical Review B* **105**, 155140 (2022).
- ⁴⁷ H. Soifer, A. Gauthier, A. F. Kemper, C. R. Rotundu, S.-L. Yang, H. Xiong, D. Lu, M. Hashimoto, P. S. Kirchmann, J. A. Sobota, et al., *Physical Review Letters* **122**, 167401 (2019).
- ⁴⁸ A. Bharti, M. Ivanov, and G. Dixit, *Physical Review B* **108**, L020305 (2023).
- ⁴⁹ N. Rana and G. Dixit, *Physical Review Applied* **19**, 034056 (2023).
- ⁵⁰ M. Mrudul, Á. Jiménez-Galán, M. Ivanov, and G. Dixit, *Optica* **8**, 422 (2021).
- ⁵¹ M. Mrudul and G. Dixit, *Journal of Physics B* **54**, 224001 (2021).